This is a repository copy of *Evaporation/boiling heat transfer characteristics in an artery porous structure*.

Article:

Experimental study on the supercritical startup of cryogenic loop heat pipes with redundancy design

Yuandong Guo[1],   Guiping Lin[1],   Lizhan Bai[1,3,*],   Xueqin Bu[1],

Hongxing Zhang[2],   Jiang He[2],   Jianyin Miao[2],   Dongsheng Wen[3]

1 Laboratory of Fundamental Science on Ergonomics and Environmental Control, School of Aeronautic Science and Engineering, Beihang University, Beijing 100191, PR China

2 Beijing Key Laboratory of Space Thermal Control Technology, Beijing Institute of Spacecraft System Engineering, China Academy of Space Technology, Beijing 100094, PR China

3 School of Chemical and Process Engineering, University of Leeds, Leeds, LS2 9JT, UK

Abstract: Cryogenic loop heat pipe (CLHP) is one of the key components in the future space infrared exploration system, which enables effective and efficient cryogenic heat transport over a long distance with a flexible thermal link. To realize reliable and long life operation, a CLHP-based thermal control system with redundancy design was proposed in this work, where two nitrogen-charged CLHPs were employed to provide cryocooling at 80-100K. This study focused on the supercritical startup of the CLHPs with redundancy design, and an extensive experimental study under four possible working modes was conducted. Experimental results showed that with 2.5W applied to the secondary evaporator, each CLHP could realize the supercritical startup successfully in the normal working mode; however, the required time differed a lot because the difference in the transport line diameter significantly affected the cryocooling capacity to the primary evaporator. In the backup conversion mode, instant switch of the two primary evaporators may cause an operation failure, and an auxiliary operation of the secondary evaporator in advance was necessary to make the primary liquid line filled with liquid. In the malfunction conversion mode, the simulated infrared detector had to be first shut down, but the time needed for the backup CLHP to realize the supercritical startup became obviously shorter than that in the normal working mode, because the primary evaporator of the backup CLHP was always in a cryogenic state. In the dual operation mode, the two CLHPs could realize the supercritical startup simultaneously, but a temperature oscillation phenomenon was observed, which can be eliminated by increasing the heat load applied to the secondary evaporator.

Keywords: loop heat pipe; cryogenic; supercritical startup; working mode; experiment

---

* Corresponding author. Tel.: +86 10 8233 8600; Fax: +86 10 8233 8600.

E-mail address: bailizhan@buaa.edu.cn (L. Bai).

1 Introduction

Heat pipe is an advanced two-phase heat transfer device, which combines the principles of both thermal conduction and liquid/vapor phase change to efficiently manage the heat transfer processes between two solid interfaces, and its operating principle, performance and characteristics were detailed in Refs.[1, 2]. Since the first basic concept of heat pipe was proposed by Gaugler [3], it has attracted the interests of researchers worldwide, and various types of heat pipes operating at different temperature ranges have been developed to satisfy specific application requirements [4-7]. So far, heat pipes have been applied in a variety of areas in both space and terrestrial surroundings such as in the building natural ventilation system, electronics cooling, industrial waste heat recovery and spacecraft thermal control [8-13].

As one of the latest developments of the heat pipe technology, cryogenic loop heat pipe (CLHP) can realize efficient heat transport at the cryogenic temperatures. Depending on the working fluids charged, CLHPs can operate in a specific low temperature range, i.e., propane for the operating temperature range of 200-240 K, oxygen for 90-140 K, nitrogen for 80-110 K, neon for 30-40 K and hydrogen for 20-30 K, and when helium is selected as the working fluid, the operating temperature can be reached as low as 2-4 K. Compared with traditional cryogenic heat pipes, CLHP exhibits a variety of advantages such as higher heat transfer capacity, longer heat transport distance and stronger antigravity capability, as well as good flexibility for complex structures. An important example for the CLHP applications is in the thermal control of the space infrared exploration system where the infrared sensors/detectors have to be maintained at 80-100 K or even lower temperatures [14, 15].

For ambient loop heat pipe, the working fluids charged are typically ammonia, acetone, water, etc., which are in the two-phase state at ambient temperature. Because the evaporator wick is always saturated by the liquid through the matching design of the compensation chamber volume and the working fluid inventory, heat load can be applied to the evaporator immediately to initiate the startup. However, for CLHP, the situation becomes much

2

different. Because the critical temperatures of the cryogenic working fluids are much lower than the ambient

temperature, i.e., the critical temperature of nitrogen is about 126 K, and the cryogenic working fluids are in the

supercritical state at ambient temperature. In order to start up the CLHP, prior to the application of heat load to the

evaporator, the working fluid inside must be first cooled to below its critical temperature until it condenses and

saturates the evaporator wick, and an auxiliary measure will be needed to help realize the liquid saturation of the

evaporator wick [16]. From the above analysis, a CLHP will inevitably experience a supercritical startup to realize

the normal operation.

So far, several types of CLHPs employing different auxiliary measures to realize the supercritical startup have

been developed, such as the gravity-assisted method [16], the secondary evaporator method [17-22], the auxiliary

loop method [23-28] and the capillary pump method [29-30], as reviewed in our previous paper [31]. Because the

CLHP employing the auxiliary loop method can realize the supercritical startup in space microgravity

environment, and can manage the parasitic heat load effectively with a relatively high heat transport capacity, it is

the most suitable for space applications and is selected as the object of study in this work. Below provides a brief

review on the development of this type of CLHP.

James et al. [23] proposed an ethane-charged CLHP operating at a temperature range of 215-218K for passive

optical bench cooling applications. Experimental results showed that the CLHP could reliably realize the

supercritical startup from an initially supercritical temperature of 335K with a heat load of 60W applied to the

secondary evaporator,. With a heat load of 5W applied to the secondary evaporator to manage the parasitic heat

load, the CLHP achieved a 50W heat transport capability at 215K. Hoang et al. [14] developed a nitrogen-charged

CLHP operating in a temperature range of 80-110K for across-gimbal cryocooling, which could successfully

realize the supercritical startup from an initially supercritical temperature of 298K, with a heat load of 5W applied

to the secondary evaporator. The maximum heat transport capability was determined to be 5W over a transport

73   distance of 4.3m. Later, a hydrogen-charged CLHP with a swing volume design was experimentally studied to

74   reduce the system volume/weight. The CLHP could realize the supercritical startup with a heat load of 2.5W

75   applied to the secondary evaporator when the shroud temperature was 200K; however, a supercritical startup

76   failure occurred in a 298K environment due to large parasitic heat load. The CLHP could operate at a temperature

77   range of 20-30K, and a maximum heat transport capability of 10W over a transport distance of 2.5m was obtained

78   with a 80K shroud [15]. To solve important problems in cryogenic integration, Bugby et al. [24, 25] developed

79   three CLHPs: an across-gimbal CLHP, a short and a long transport length miniaturized CLHP. The across-gimbal

80   CLHP employed nitrogen as the working fluid with a heat transport range of 2-20W. Both the short and long

81   transport length CLHPs utilized neon as the working fluid and operated at a temperature range of 30-40K.

82   Preliminary test results showed that the short and long transport length CLHPs were able to transport a heat load

83   of 0.1-2.5W and 0.1-0.8 W respectively. Gully et al. [26] designed and experimentally studied a nitrogen-charged

84   CLHP, where the effects of heat load, charged pressure and radiation heat load were studied in steady state

85   operation, and a maximum heat load of 19W was achieved over a transport distance of 0.5m. All the CLHPs

86   mentioned above employed a single-tube condenser where the flow resistance is relatively large. In order to

87   reduce the flow resistance in the condenser and increase the heat transport capacity of CLHPs, Zhao et al. [27, 28]

88   first proposed a nitrogen-charged CLHP with a parallel condenser design. Experimental results confirmed that the

89   CLHP could operate with a high heat transfer capacity up to 41W across a 0.48m transport distance.

90   From the above review, it is clear that CLHP is an effective and efficient cryogenic heat transport device with

91   many potential cryogenic applications. However, most current studies are still in the proof-of-concept stage,

92   where proper design of the evaporator and condenser structures to satisfy the connection requirements with the

93   heat source and heat sink has not been considered. At the same time, for space applications especially for the

94   space infrared exploration system, a miniaturization design with reduced system volume/weight should be

95 conducted. Besides these aspects, high reliability and long life design is of high priority, because the design life of

96 the next generation infrared observation satellites is over ten years or even longer, and on-orbit maintenance is

97 generally impossible for most space missions. Although there is no moving parts in the CLHPs, which promises a

98 long life nature, however, learning from the experience of applying ambient loop heat pipes in the spacecraft

99 thermal control system, it is possible that the operation anomaly or failure may occur for the loop heat pipes under

100 orbital conditions occasionally. For instance, for the spacecraft TacSat 4 launched in 2011, the Central Thermal

101 Bus design of the thermal control system utilized an ambient loop heat pipe to acquire/transport waste heat from

102 the on-board electronics and reject it to space via radiator panels. After a period of operation, operation anomaly

103 occurred for the loop heat pipe, resulted in much degraded performance of the thermal control system [32].

104 Several years ago, operation anomaly also occurred for a loop heat pipe applied in the thermal control system of

105 the Geoscience Laser Altimetry System on the ICESat Satellite [33]. Therefore, it is quite necessary to adopt the

106 redundancy design to improve the operation reliability and realize a long life operation.

107   In order to address these issues and promote the future space applications of CLHPs , a CLHP-based thermal

108 control system with redundancy design was proposed in this work, where a miniature nitrogen-charged CLHP was

109 designed and fabricated considering appropriate interfaces with the heat source and heat sink, i.e., a saddle design

110 was used to realize easy connection between the cylindrical evaporator and simulated infrared detector, and a

111 novel cylindrical condenser design provided convenient interface with the cold finger of a pulse tube refrigerator.

112 To the best of our knowledge, this is the first experimental study on the CLHPs with redundancy design, and here

113 we mainly focus on the supercritical startup process, which is a very complicated but indispensable process prior

114 to the attainment of normal operation for CLHPs. Different working modes for the supercritical startup have been

115 defined due to the adoption of redundancy design, and extensive experimental studies were conducted, as

116 described in detail below.

117   **2 Experimental setup**

118   Fig. 1 shows the schematic view of the experimental rig in this work, which was comprised of two CLHPs, a

119   heating system, a cryogenic cooling system, a temperature measurement and data acquisition system and a

120   thermal-vacuum chamber. Fig. 2 shows the CLHP-based thermal control system with redundancy design where

121   the two CLHPs (#1 and #2) were connected with a pulse tube refrigerator respectively, and Fig. 3 shows the photo

122   of the CLHPs in the experiment. Because the CLHPs both employed an auxiliary loop to help realize the

123   supercritical startup, it was composed of a main loop and a secondary loop in addition to a gas reservoir. The main

124   loop included a primary evaporator, a primary CC (compensation chamber), a primary condenser and primary

125   vapor and liquid lines. The secondary loop consisted of a secondary evaporator, a secondary CC, a secondary

126   condenser and secondary loop lines. The gas reservoir with a comparatively large volume was utilized to reduce

127   the system pressure at ambient state, and it was connected to the inlet of the primary condenser. All the

128   components of the CLHP were made of stainless steel except that the primary and secondary evaporator wicks

129   were made of sintered nickel powders. The operating temperature of the CLHPs was designed in the range of

130   80-100 K, and nitrogen whose purity was greater than 99.9995% was charged as the working fluid. Table 1

131   presents the basic parameters of the CLHPs, where CC represents the compensation chamber and OD and ID

132   represent the outer and inner diameters respectively.

133   To realize the redundancy design, the primary evaporators of the two CLHPs were coupled to a copper saddle,

134   as shown in Fig. 4, and a thin-film electric resistance heater was directly attached to the copper plate to simulate

135   the heat generated from a space infrared detector. The heat load of the electric heater can be adjusted from 0 to

136   30W by altering the DC power output voltage with an uncertainty of ±5.0%, which can be transferred to both

137   primary evaporators through the copper saddle. In addition, the two secondary evaporators of the CLHPs were

138   both attached by a thin-film electric resistance heater respectively to provide auxiliary heat loads during the

139 supercritical startup. Two pulse tube refrigerators were employed as the cryogenic heat sink, whose cold fingers

140 were connected with the two cylindrical primary condensers of the CLHPs respectively. The pulse tube

141 refrigerator is a refrigeration device based on the Simon expansion principle to obtain the cooling effect through

142 charging and discharging high purity helium gas in the pulse tube. It was composed of a cold finger, a compressor

143 and a controller, with a cooling capacity greater than 4W at 70K. The pulse tube cold finger and the compressor

144 made up the main body, and the controller modulate the input power for its operation. In the operation, the

145 compressor can produce continuous sinusoidal pressure fluctuations, and the refrigerant gas experiences

146 endothermic expansion at the low temperature side and exothermic compression at the high temperature side, to

147 achieve the cooling effect through the phase modulation mechanism.

148   To reduce the parasitic heat load from the ambient surroundings, the CLHPs were placed in a thermal-vacuum

149 chamber, and all the components except the gas reservoir were covered with multilayer insulation materials. As

150 the pressure in the thermal-vacuum chamber can be maintained always below 1×10^{-3} Pa, the parasitic heat load by

151 convective heat transfer becomes very small and can be safely neglected. Calibrated Type T thermocouples (TCs)

152 with measuring uncertainties of ±1.0 K were used to monitor the temperature variations of some characteristic

153 points along the loop, as shown in Fig. 5. To reduce the influence of gravity, the primary evaporator and the

154 primary condenser of the two CLHPs were always placed in a horizontal plane in the experiments.

155 **3 Definition of different working modes**

156   For a CLHP-based thermal control system with a redundancy design, it is expected that there are four possible

157 working modes: the normal working mode, the backup conversion mode, the malfunction conversion mode and

158 the dual operation mode, which covers the system operation in the whole lifetime. In the normal working mode,

159 only one CLHP with the connected pulse tube refrigerator is operating to provide cryocooling to the infrared

160 detector, while the other one is in the idle state. The backup conversion mode means to start up the CLHP in the

idle state and shut down the other one in operation to realize a smooth switch of the operation between the two

CLHPs, while maintaining the infrared detector at the normal working state. The malfunction conversion mode

means when the pulse tube refrigerator in operation breaks down or other similar issues emerge, it is necessary to

start up the other CLHP in the idle state to provide sufficient cryocooling. Under this condition, the infrared

detector in operation must be first shut down before the completion of the supercritical startup of the other CLHP.

At the end of the lifetime of the thermal control system, the cryocooling provided by a single one pulse tube

refrigerator may be insufficient due to the performance degradation after several years of operation. Under such a

condition, both CLHPs with their corresponding pulse tube refrigerators will be needed to operate simultaneously,

so as to provide sufficient cryocooling, which is termed as the dual operation mode. This working mode is of great

importance to guarantee the normal operation of the space infrared exploration system at the end of lifetime.

4 Experimental results and analysis

4.1 Normal working mode

Fig. 6(a) shows the temperature variations of some characteristic points along the loop during the supercritical

startup of the #1 CLHP. As shown in Fig. 6(a), the supercritical startup was initiated from an initially supercritical

temperature of about 300K. At 22 min, the cold finger of the pulse tube refrigerator began to take effect, and the

temperatures at the secondary evaporator (TC10) and at the outlet of the primary condenser (TC7) dropped rapidly,

due to direct contact with the cold finger of the refrigerator. At 50 min, the temperatures at the secondary

evaporator, secondary evaporator outlet and primary condenser outlet dropped at a much faster rate, indicating

that the temperatures of nitrogen gas in the primary condenser and secondary CC dropped to their saturation

temperatures corresponding to the local pressure, and fluid condensation occurred there afterwards, making the

heat transfer proceed in a more efficient way. Several minutes later, the temperatures at the secondary evaporator

(TC10) and at the primary condenser outlet (TC7) began to drop slowly and remained at about 90 K, indicating

that nitrogen in the two-phase state began to exist there. As time went by, the inventory of liquid nitrogen in the

secondary evaporator would increase gradually, and it would fully saturate the secondary evaporator wick

eventually. At 60 min, a very large temperature drop occurred at the primary CC inlet (TC1) due to the arrival of

the condensate from the primary condenser, from which it can be inferred that when the secondary CC was cooled,

the temperature/pressure of the working fluid inside it dropped, and a fluid circulation from the gas reservoir

through the primary condenser, primary liquid line and the secondary loop line to the secondary CC should exist,

to continuously supply working fluid to the secondary CC.

With the temperature of the secondary evaporator remaining at 90 K for about 12 min, a heat load of 2.5W was

applied to the secondary evaporator ($Q_{se}^{(1)}$), and no obvious temperature rise of the secondary evaporator (TC10)

was observed, indicating that the secondary evaporator was started up successfully. Under such a condition, the

secondary evaporator could act as a pump to drive the condensed liquid nitrogen in the primary condenser to the

primary evaporator core and CC through the primary liquid line (path 1), as evidenced by continous temperature

drop at the outlet of the primary CC (TC8), at the primary evaporator (TC3) and at the primary evaporator outlet

(TC4). Note that, there was another flow path from the secondary evaporator to the primary evaporator core, i.e.

from the secondary evaporator through the primary vapor line, primary evaporator vapor grooves and primary

evaporator wick to the primary evaporator core (path 2). Because of the difference in flow resistance between the

two paths from the secondary evaporator to the primary evaporator core, more than 80% of the heat load on the

secondary evaporator would flow through the path 1. As the primary evaporator wick began to be saturated with

liquid coming from the primary condenser, the capillary pressure developed by the primary evaporator wick

would totally shut down path 2 and force all the heat load on the secondary evaporator to flow through the path 1,

resulted in a more efficient cooling to the primary evaporator. This was evidenced by more rapid cooldown rate of

the primary evaporator and a sudden temperature drop at the primary evaporator outlet (TC4) at about 150 min.

205   With the operation of the secondary evaporator for about 90 min, the primary evaporator temperature (TC3)

206   dropped to about 90K and began to remain unchanged, indicating that nitrogen in the two-phase state began to

207   exist in the primary evaporator wick. As time went by, the inventory of liquid nitrogen in the primary evaporator

208   would increase gradually and fully saturate the primary evaporator wick eventually. With the primary evaporator

209   temperature remaining at 90K for several minutes, a heat load of 1W was applied to the copper saddle (Q_{cs}), and

210   the heat load applied to the secondary evaporator ($Q_{se}^{(1)}$) was reduced to 1W. No obvious temperature rise of the

211   primary evaporator was observed, indicating that the primary evaporator was started up successfully. With the

212   normal operation of the primary evaporator, the #1 CLHP realized the supercritical startup.

213   Fig. 6 (b) shows the temperature variations of some characteristic points along the loop during the supercritical

214   startup of the #2 CLHP, which were similar to those of #1 CLHP during the whole supercritical startup process.

215   However, in Fig. 6(b), the secondary evaporator had to operate for about 240 min with a heat load of 2.5W ($Q_{se}^{(2)}$)

216   to realize the large temperature drop of the primary evaporator from the ambient state (300K) to the saturation

217   temperature (90K), which became much longer than that of #1 CLHP (90 min). This phenomenon can be

218   explained according to the difference in the structural size between the two CLHPs: because the inner diameter of

219   the liquid line of #2 CLHP (1.0mm) is much smaller than that of #1 CLHP (2.0mm), the flow resistance in the

220   liquid line of #2 CLHP becomes much larger. As discussed above, there are two paths from the secondary

221   evaporator to the primary evaporator core, and only for path 1, the condensate in the primary condenser can be

222   driven into the primary evaporator core with a much larger cryocooling capacity; at the same time, the

223   cryocooling capacity is strongly dependent on the mass flowrate of the working fluid in path 1. For #2 CLHP, the

224   considerably increased flow resistance in the primary liquid line changes the balance of the flow resistance

225   between the two paths, which leads to much reduced mass flowrate in path 1, compared to the situation in #1

226   CLHP. Therefore a careful flow resistance analysis should be conducted in the CLHP design to effectively

227 accelerate the supercritical startup process.

228 **4.2 Backup conversion mode**

229   In the backup conversion mode, a smooth switch of the operation of the two primary evaporators will be

230 completed while the infrared detector always keeps working, and the two pulse tube refrigerators have to be

231 operating simultaneously for a period of time. Because the coefficient of performance (COP) of the pulse tube

232 refrigerator is only 2.0% or even lower when it is operating at a cryogenic temperature range of 80-100K, it is a

233 high energy-consuming component in the thermal control system. As the space power supply is limited, it is very

234 important to accelerate the backup conversion by reducing the time of simultaneous operation of the two pulse

235 tube refrigerators for the energy saving purpose.

236 **4.2.1 Backup conversion without auxiliary operation**

237   In order to reduce the backup conversion time maximally, backup conversion from #1 to #2 CLHP without an

238 auxiliary operation of the secondary evaporator in advance was first experimentally studied, as shown in Fig. 7,

239 where an operation failure occurred.   At the initial state, the #1 CLHP was in normal operation with a heat load

240 of 4W and 0.5W applied to the copper saddle and secondary evaporator respectively. At about 15 min, #2 pulse

241 tube refrigerator was started, and the temperatures of the primary condenser (TC17) and secondary evaporator

242 (TC21) of the #2 CLHP began to drop gradually. At about 70 min, the temperature of the secondary evaporator

243 (TC21) of the #2 CLHP had dropped to the saturation temperature (90K) and remained at this value for several

244 minutes, indicating that nitrogen in the two-phase state began to exist there and liquid nitrogen would saturate the

245 secondary evaporator wick eventually. Then the #1 pulse tube refrigerator and heat load applied to the secondary

246 evaporator of the #1 CLHP was turned off, and a heat load of 0.5W was applied to the secondary evaporator of the

247 #2 CLHP simultaneously, trying to realize an instant switch of the operation of the two primary evaporators. The

248 primary evaporator temperature of the #2 CLHP (TC14) began to rise continuously, indicating that an operation

249 failure occurred.

250   The reason for the operation failure was analyzed below. After the #1 CLHP with the connected #1 pulse tube

251 refrigerator was totally shut down, a heat load of 4W and 0.5W was actually applied to the primary and secondary

252 evaporators of the #2 CLHP respectively. Although the primary and secondary evaporator wicks of the #2 CLHP

253 had been saturated by the liquid nitrogen, the working fluid in the primary liquid line was still in the vapor state

254 with a relatively high temperature. With the circulation of the working fluid in the primary loop of the #2 CLHP,

255 the nitrogen vapor in the primary liquid line was pushed into the primary evaporator core, thus causing

256 insufficient liquid supply to the primary evaporator wick, and the normal operation would be interrupted

257 accompanied by a continuous temperature rise of the primary evaporator of the #2 CLHP.

258 **4.2.2 Backup conversion with auxiliary operation**

259   In order to address the above issue and ensure a successful backup conversion, in the subsequent experiment, an

260 auxiliary operation of the secondary evaporator of the #2 CLHP with a heat load of 2.5W was first implemented

261 before the total shut down of the #1 CLHP with the connected #1 pulse tube refrigerator, to guarantee that the

262 primary liquid line of the #2 CLHP was filled with liquid nitrogen prior to the startup of the primary evaporator.

263   As shown in Fig. 8, after the secondary evaporator wick of the #2 CLHP was fully saturated by the liquid

264 nitrogen, different from the case in Fig. 7, a heat load of 2.5W was first applied to the secondary evaporator to

265 start up the secondary loop, before the total shut down of the #1 CLHP with the #1 pulse tube refrigerator, With

266 the circulation of the working fluid in the secondary loop of the #2 CLHP for about 10 minutes, the primary liquid

267 line would be filled with liquid nitrogen, under such a condition, it was ready to start up the primary loop of the #2

268 CLHP. At about 102 min, the #1 pulse tube refrigerator and heat load applied to the secondary evaporator of the

269 #1 CLHP was turned off, and a reduced heat load of 0.5W was applied to the secondary evaporator of the #2

270 CLHP simultaneously, to realize a switch of the operation of the two primary evaporators. It was as expected that

no obvious temperature rise of the primary evaporator of the #2 CLHP (TC14) was observed, indicating that a

successful backup conversion was achieved.

In the backup conversion mode, because the primary evaporator of the backup CLHP has already been filled

with liquid nitrogen, the purpose for the auxiliary operation of the secondary evaporator is only to make the

primary liquid line flooded by the liquid nitrogen, and the time needed for the auxiliary operation of the secondary

evaporator is remarkably reduced compared with the case in the normal working mode.

4.3 Malfunction conversion mode

Fig. 9 shows the temperature variations of some characteristic points along the loop during the supercritical

startup in the malfunction conversion mode. At the initial state, the #2 CLHP was in the normal operation with a

heat load of 4W and 0.5W applied to the copper saddle and secondary evaporator respectively. At 25 min, #2 pulse

tube refrigerator was shut down to simulate the operation failure in real applications. Several minutes later, a

sudden temperature drop occurred at the outlet of the primary evaporator of the #1 CLHP, indicating that a certain

amount of heat load applied to the copper saddle was transferred to the primary evaporator of the #1 CLHP where

vapor was generated and flowed out of the primary evaporator. At 30 min, it was found that the primary

evaporator temperature of the #2 CLHP (TC14) rose quickly, indicating that an operation failure occurred for the

thermal control system, then the heat load applied to the copper saddle was turned off, and the #1 pulse tube

refrigerator was started to initiate a malfunction conversion.

As shown in Fig. 9, the supercritical startup process of the #1 CLHP is similar to that in Fig. 6(a); however, the

time needed for the auxiliary operation of the secondary evaporator was reduced remarkably, i.e., in Fig. 6(a), the

secondary evaporator had to operate for about 90 minutes to realize the cryocooling to the primary evaporator,

while here only 40 minutes was needed, that was because the primary evaporator of the backup CLHP (#1 CLHP)

was always in a cryogenic state, and the cryocooling needed to realize the liquid saturation of the primary

293   evaporator wick decreased considerably. In the malfunction conversion mode, the simulated infrared detector had

294   to be shut down for about 120 minutes.

295   **4.4 Dual operation mode**

296   Fig. 10 shows the temperature variations of some characteristic points along the loop during the supercritical

297   startup of the two CLHPs. As shown in Fig. 10, at the initial state, all the characteristic points along the loop were

298   at the ambient temperature of about 295 K, and the supercritical startup of the two CLHPs was initiated

299   simultaneously. After the secondary evaporator wicks of the two CLHPs were fully saturated by the liquid, a heat

300   load of 2.5W was applied to the secondary evaporators of the two CLHPs respectively to start up the secondary

301   loop. After the primary evaporator wicks of the two CLHPs were fully saturated by the liquid, a heat load of 4W

302   was applied to the copper saddle, and the heat loads applied to the secondary evaporators were both reduced to 1W.

303   No obvious temperature rise of each primary evaporator was observed, indicating that the normal operation for

304   each CLHP was established, and successful supercritical startup of the two CLHPs in dual operation mode was

305   achieved. During the supercritical startup, it took about 120 minutes for the auxiliary operation of the secondary

306   evaporators to realize the cryocooling to the two primary evaporators from an ambient temperature (295K) to their

307   saturation temperature (90K), which was between the times required by #1 and #2 CLHPs in the normal working

308   mode, i.e., 90 and 240 minutes respectively, indicating that heat transfer between the #1 and #2 primary

309   evaporators through the copper block should exist to help the #2 primary evaporator to accelerate the temperature

310   drop process.

311   In the dual operation mode, obvious temperature oscillation phenomenon was observed for the #1CLHP when

312   the heat load applied to the secondary evaporator was relatively small. As shown in Fig. 11, when the heat load

313   applied to the secondary evaporator of the #1CLHP was 1W, obvious temperature oscillation at the inlets of the

314   primary CC (TC1) and the primary condenser (TC5) was observed; however, when the heat load applied to the

14

secondary evaporator was increased to 1.5W, the temperature oscillation phenomenon would disappear completely. This phenomenon may be explained as follows: when the heat load applied to the secondary evaporator is relatively small, the total mass flowrate in the primary liquid line was small accordingly, and the return subcooling may be insufficient to offset the heat leak to the primary CC from both the primary evaporator and the ambient surroundings, causing an increase of the temperature/pressure in the primary CC and resultant oscillation movement of the working fluid along the main loop; however, when the heat load applied to the secondary evaporator is increased to appropriate relatively high level, the total mass flowrate in the primary liquid line increases accordingly, and the return subcooling becomes sufficient to offset the heat leak to the primary CC, under this condition, oscillation flow in the main loop will be completely impossible.

5 Conclusions

A CLHP-based thermal control system with redundancy design for future space infrared exploration system was designed and fabricated, and an extensive experimental study on the supercritical startup characteristics under four possible working modes was conducted, where the temperature variations of some characteristic points along the loop were presented, and the mechanisms responsible for specific phenomenon were analyzed. According to the experimental results, important conclusions have been reached as summarized as follows:

◆ In the normal working mode, with 2.5W applied to the secondary evaporator, each CLHP could successfully realize the supercritical startup independently; however, the required time differed a lot because the difference in the transport line diameter significantly affected the cryocooling capacity to the primary evaporator, and a smaller diameter transport line may result in a much longer supercritical startup time.

◆ In the backup conversion mode, instant switch of the two primary evaporators may cause an operation failure, and an auxiliary operation of the secondary evaporator of the backup CLHP in advance was necessary to make the primary liquid line filled with liquid and ensure a successful backup conversion.

337 ◆ In the malfunction conversion mode, the simulated infrared detector had to be first shut down, but the time

338 needed for the backup CLHP to realize the supercritical startup become obviously shorter than that in the

339 normal working mode because the primary evaporator of the backup CLHP was always in a cryogenic state,

340 and the cryocooling needed to realize the liquid saturation of the primary evaporator wick decreased

341 considerably.

342 ◆ In the dual operation mode, the two CLHPs could realize the supercritical startup simultaneously, and the

343 time needed was between the ones required by the two CLHPs in the normal working mode, due to the heat

344 transfer between the two primary evaporators through the copper saddle; however, a temperature oscillation

345 phenomenon was observed, which can be eliminated effectively by increasing the heat loads applied to the

346 secondary evaporator.

347 As the first reported experimental study on a CLHP-based thermal control system with redundancy design, the

348 experimental results and analysis provided here contribute greatly to the design and future space applications of

349 such an advanced thermal control system with high reliability and long lifespan.

356

357   **References**

358   [1]   G.P. Peterson, An introduction to heat pipes, 1st ed. Singapore: John Wiley & Sons, Inc., 1994

359   [2]   A. Faghri, Heat pipe science and technology, 1st ed. London: Taylor & Francis, Inc., 1995

360   [3]   R.S. Gaugler, Heat transfer device, U.S. Patent No. 2350 348, 1944

361   [4]   S. Hong, X. Zhang, Y. Tang, et al., Experiment research on the effect of the evaporator's configuration design of an innovative

362   ultra-thin looped heat pipe, International Journal of Heat and Mass Transfer 92(2016) 497-506

363   [5]   Y. F. Maydanik, Loop heat pipes, Applied Thermal Engineering 25 (2005) 635-657

364   [6]   L. Bai, G. Lin, D. Wen, et al. Experimental investigation of startup behaviors of a dual compensation chamber loop heat pipe

365   with insufficient fluid inventory, Applied Thermal Engineering 29 (2009)1447-1456

366   [7]   T. Tharayil, L.G. Asirvatham, V. Ravindran, et al., Thermal performance of miniature loop heat pipe with graphene-water

367   nanofluid, International Journal of Heat and Mass Transfer, 93(2016) 957-968

368   [8]   Yuechao Deng, Zhenhua Quan，Yaohua Zhao，et al., Experimental research on the performance of household-type

369   photovoltaic-thermal system based on micro-heat-pipe array in Beijing, Energy Conversion and Management

370   106(2015)1039-1047

371   [9]   M.S. Naghavi, K.S. Ong, M. Mehrali, et al., A state-of-the-art review on hybrid heat pipe latent heat storage systems, Energy

372   Conversion and Management 105(2015) 1178-1204

373   [10]   H. Jafari Mosleh, S. Jahangiri Mamouri, M.B. Shafii, et al., A new desalination system using a combination of heat pipe,

374   evacuated tube and parabolic trough collector, Energy Conversion and Management 99 (2015)141-150

375   [11]   R. M. Fairuz, D. Abhijit, O. Bradley, et al., Experimental investigation of combined heat recovery and power generation using

376   a heat pipe assisted thermoelectric generator system, Energy Conversion and Management, 111(2016) 147-157

377   [12]   K. Nithyanandam and R. Pitchumani, Design of a latent thermal energy storage system with embedded heat pipes, Applied

378   Energy 126(2014) 266-280

379   [13]   Kai-Shing Yang, Tsung-Yi Yang, Cheng-Wei Tu, et al., A novel flat polymer heat pipe with thermal via for cooling electronic

380   devices, Energy Conversion and Management 100 (2015) 37-44

381   [14]   T.T. Hoang, T.A. O'Connell. Performance demonstration of flexible advanced loop heat pipe for across-gimbal cryocooling.

382   AIAA paper, No.2005-5590, 2005

383   [15]   T.T. Hoang, T.A. O'Connell, J. Ku, et al. Performance Demonstration of a Hydrogen Advanced Loop Heat Pipe for 20-30K

384   Cryocooling of Far Infrared Sensors. Proceedings of SPIE 5904(2005) No.590410

385   [16]   H. Pereira, F. Haug, P. Silva, et al, Cryogenic loop heat pipes for the cooling of small particle detectors at CERN, Advances in

386   Cryogenic Engineering: Transactions of the Cryogenic Engineering Conference 55(2010) 1039-1046

387   [17]   D. Khrustalev, S. Semenov, Advances in Low-Temperature, Cryogenic and Miniature Loop Heat Pipes, Presentation at the

388   12th Annual Spacecraft Thermal Control Technology Workshop, El Segundo, March 2003

389   [18]   D. Khrustalev, Cryogenic Loop Heat Pipes as Flexible Thermal Links for Cryocoolers, Proc. of the 12th Int. Cryocooler

390   Conference, June 18-20, 2002, Cambridge, MA, USA, pp. 709-716

391   [19]   D. Khrustalev, Test Data for a Cryogenic Loop Heat Pipe Operating in the Temperature Range from 65k to 140K,

392   Presentation at the International Two-Phase Thermal Control Technology Workshop, Mitcheville, MD, September 24-26,

393   2002

394   [20]   Q. Mo, J. Liang. A novel design and experimental study of a cryogenic loop heat pipe with high heat transfer capability,

395   International Journal of Heat and Mass Transfer 49(2006) 770-776

396   [21]   Q. Mo, J. Liang, J. Cai. Investigation of the effects of three key parameters on the heat transfer capability of a CLHP,

397   Cryogenics 47(2007) 262-266

398   [22]   Q. Mo, J. Liang. Operational performance of a cryogenic loop heat pipe with insufficient working fluid inventory,

399   International Journal of Refrigeration 29(2006) 519-527

400   [23]   Y. James, E. Kroliczek，L. Crawford. Development of a Cryogenic Loop Heat Pipe (CLHP) for Passive Optical Bench

401   Cooling Applications. SAE paper, No. 2002-01-2507

402 [24] D. Bugby, B. Marland, C. Stouffer, et al., Across-gimbal and miniaturized cryogenic loop heat pipes, Space technology and

403   applications international forum-STAIF (2003) 218-226

404 [25] D. Bugby, B. Marland, C. Stouffer, et al., Development of advanced tools for cryogenic integration, Advances in Cryogenic

405   Engineering: Transactions of the Cryogenic Engineering Conference 49(2004) 1914-1922

406 [26] P. Gully, Q. Mo, T. Yan, et al. Thermal behavior of a cryogenic loop heat pipe for space application, Cryogenics 51 (2011)

407   420-428

408 [27] Y. Zhao, T. Yan, J. Liang, Experimental study on a cryogenic loop heat pipe with high heat capacity, International Journal of

409   Heat and Mass Transfer 54 (2011) 3304-3308

410 [28] T. Yan, Y. Zhao, J. Liang, et al., Investigation on optimal working fluid inventory of a cryogenic loop heat pipe, International

411   Journal of Heat and Mass Transfer 66 (2013) 334-337

412 [29] T.T. Hoang, T.A. O'Connell, J. Ku, et al., Large Area Cryocooling for Far Infrared Telescopes，Proceedings of SPIE Vol. 5172

413   (2003) 77-85

414 [30] T.T. Hoang, T.A. O'Connell, D.A. Suhkov, Large Area Cooling with Cryogenic Loop Heat Pipes, AIAA paper, No. 2007-4272,

415   2007

416 [31] L. Bai, L. Zhang, G. Lin, et al., Development of cryogenic loop heat pipes: A review and comparative analysis, Applied

417   Thermal Engineering 89(2015)180-191

418 [32] Hoang T.T., Armiger W.J., Baldauff R.W., et al. Performance of COMMx Loop Heat Pipe on TacSat 4 Spacecraft, AIAA paper,

419   No. 2012-3498, 2012

420 [33] Baker C., Butler D., Grob E., et al. Geoscience laser altimetry system (GLAS) loop heat pipe anomaly and on orbit testing,

421   AIAA paper, No. 2011-5209, 2011

422

423   **Table captions:**

424   Table1 Basic parameters of the tested CLHPs

425

426

427

428

429

430

431 **Figure captions**:
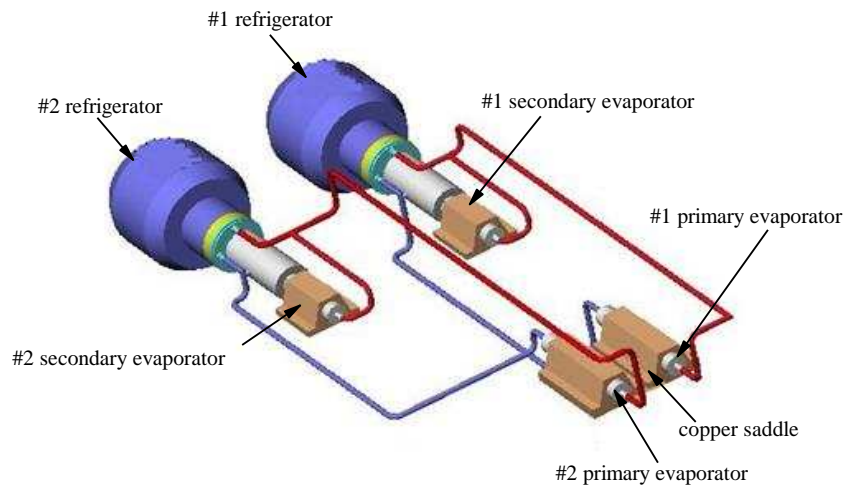
432 Fig. 1 A schematic view of the experimental system

433 Fig. 2 A schematic view of the CLHP-based thermal control system with redundancy design

434 Fig. 3 Photo of the two CLHPs in the experiment
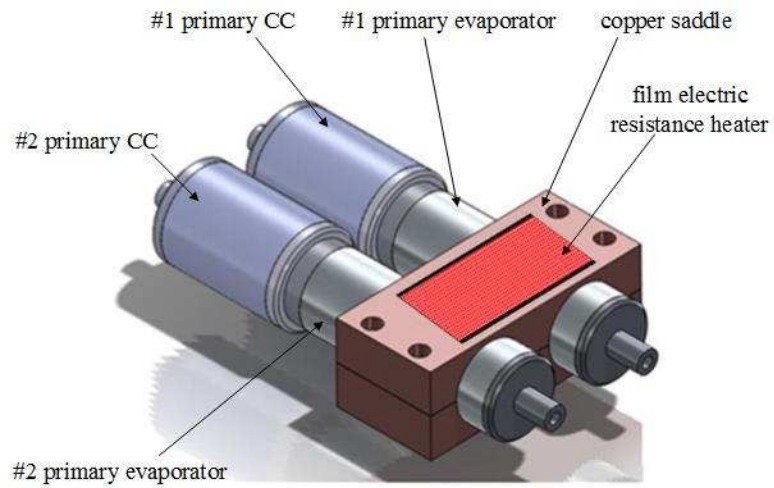
435 Fig. 4 Detailed structure of the two primary evaporators coupled by a copper saddle

436 Fig. 5 Thermocouple locations along the loop of the two CLHPs

437 Fig. 6 Supercritical startup process of the two CLHPs in the normal working mode

438 Fig. 7 Supercritical startup process without auxiliary operation in the backup conversion mode

439 Fig. 8 Supercritical startup process with auxiliary operation in the backup conversion mode

440 Fig. 9 Supercritical startup process in the malfunction conversion mode

441 Fig. 10 Supercritical startup process in the dual operation mode

442 Fig. 11 Temperature oscillation phenomenon in the dual operation mode

443

444

445

446

447

448

449

Table1 Basic parameters of the tested CLHPs

Components		Dimensions	
		#1 CLHP	#2CLHP
Primary evaporator	Casing OD/ID ×length of /mm	13×11×50	13×11×50
	Wick OD/ID ×length/mm	11×4×40	11×4×40
Secondary evaporator	Casing OD/ID ×length/mm	35×13×11	35×13×11
	Wick OD/ID ×length/mm	11×4×27	11×4×27
Primary loop	Liquid line OD/ID ×length/mm	3×2×600	2×1×600
	Condenser line OD/ID ×length/mm	2×1×700	2×1×700
	Vapor line OD/ID ×length/mm	3×2×700	3×2×700
Secondaryloop	Liquid line OD/ID ×length/mm	3×2×700	2×1×700
	Condenser line OD/ID ×length/mm	2×1×260	2×1×260
	Vapor line OD/ID ×length/mm	3×2×30	3×2×30
Wick	Maximum capillary radius/μm	0.5	0.5
	Porosity	55%	55%
	Permeability/m^2	>7×10^{-14}	>7×10^{-14}
Gas reservoir	Volume/ml	500	475

450

451

452

453

454

455

456

457

458

459
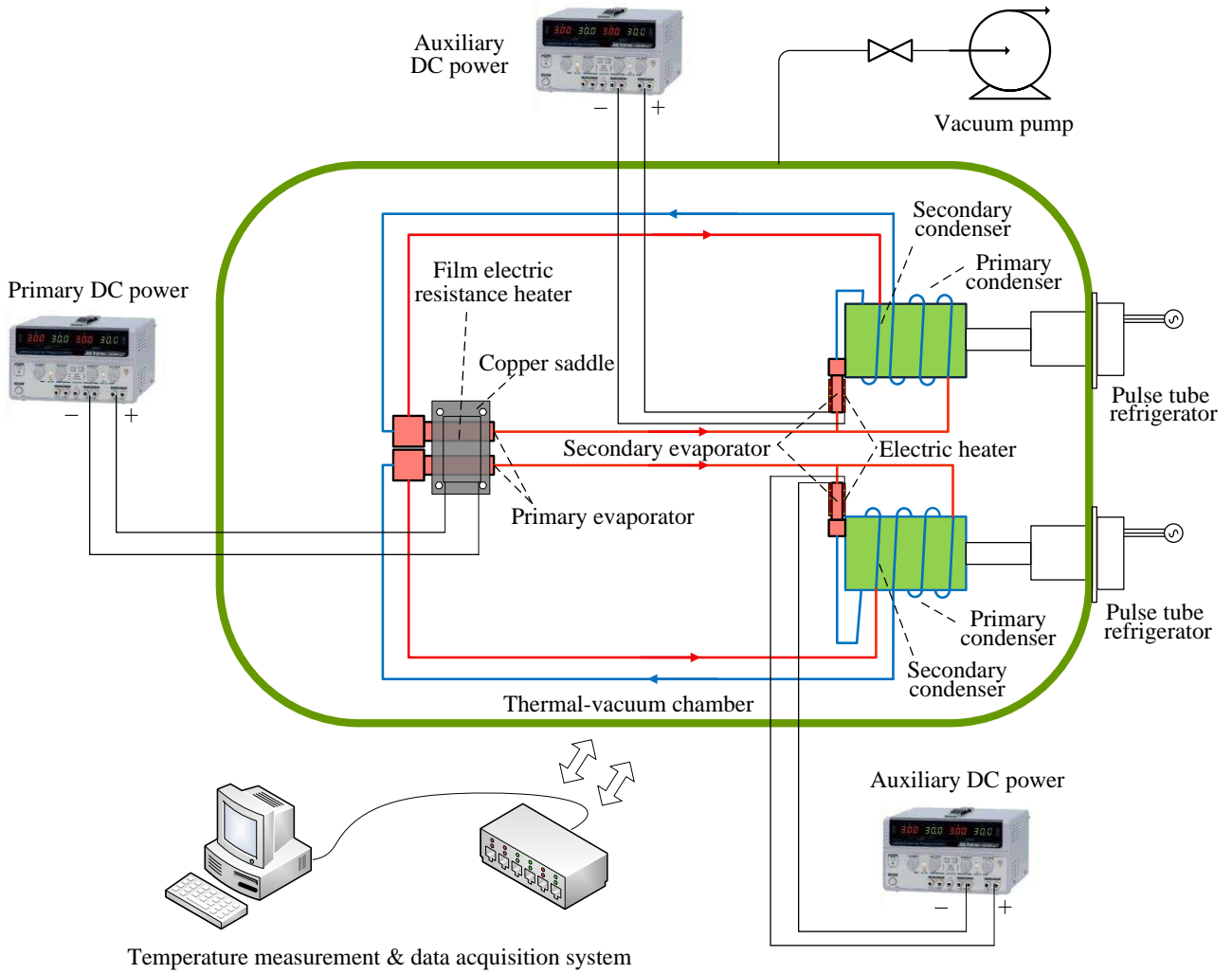
22

460

461

462

463

Fig. 1 A schematic view of the experimental system

466

467

468

469

470

471

472

473

474

Fig. 2 A schematic view of the CLHP-based thermal control system with redundancy design

477

478

479
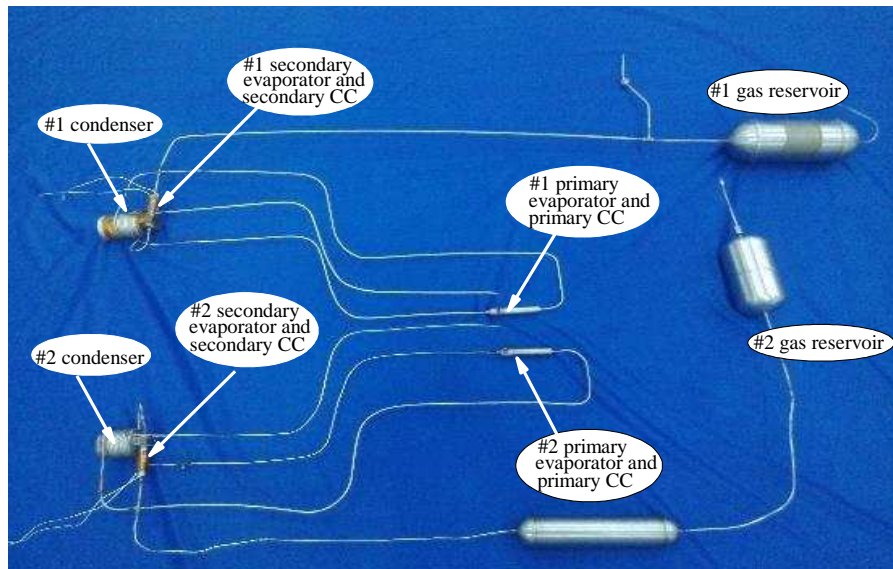
Fig. 3 Photo of the two CLHPs in the experiment

481

482

483

484

485

486

487

488

489

490

491

492

493

494

Fig. 4 Detailed structure of the two primary evaporators coupled by a copper saddle

495
496

497

498

499

500

501

502

503

504

505

506

507

508

509
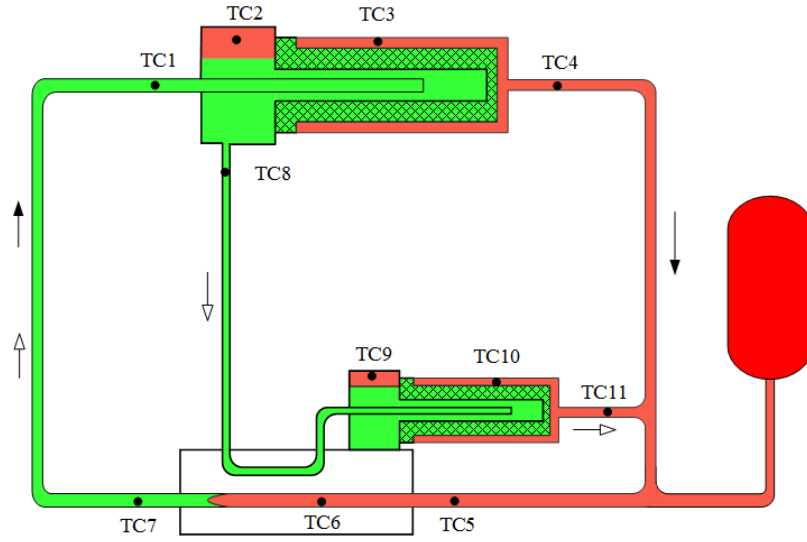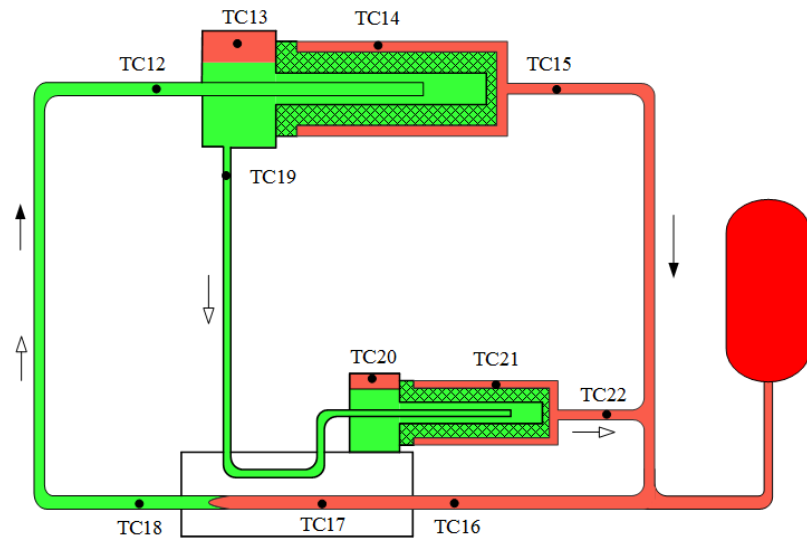
(a) #1 cryogenic loop heat pipe

510

511

(b) #2 cryogenic loop heat pipe

512

513

Fig. 5 Thermocouple locations along the loop of the two CLHPs

514

515

516

517

518

519

520

521

522
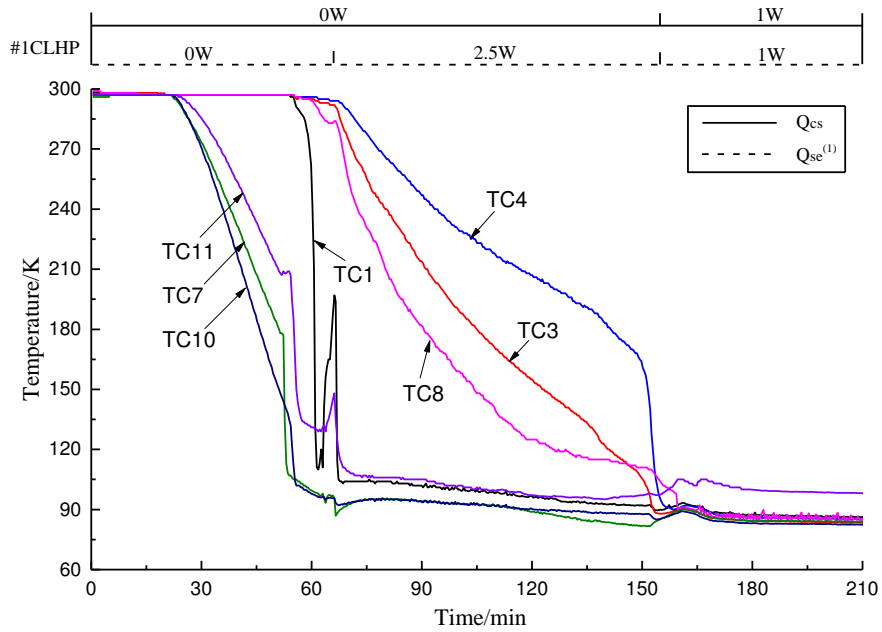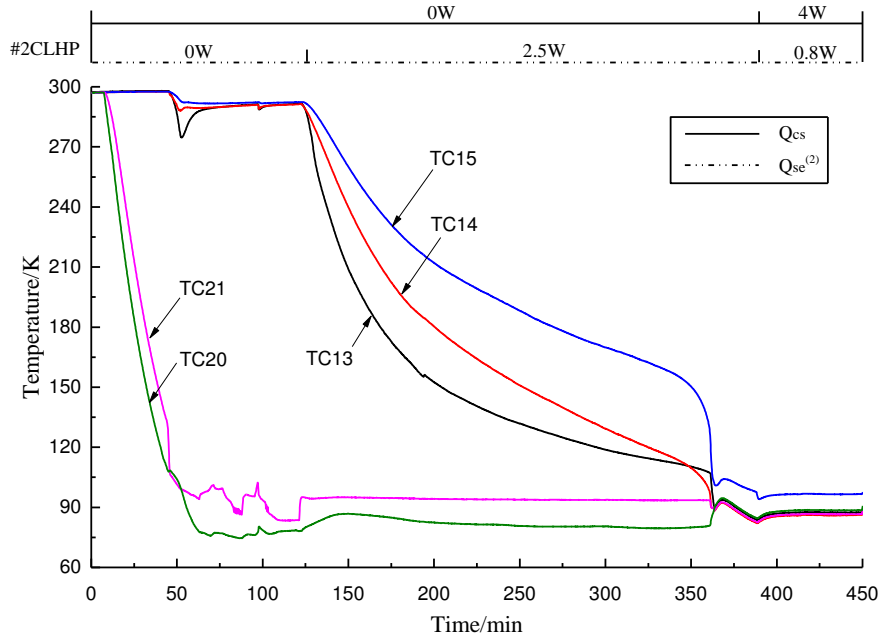
(a) #1 cryogenic loop heat pipe

(b) #2 cryogenic loop heat pipe

Fig.6 Supercritical startup process of the two CLHPs in the normal working mode
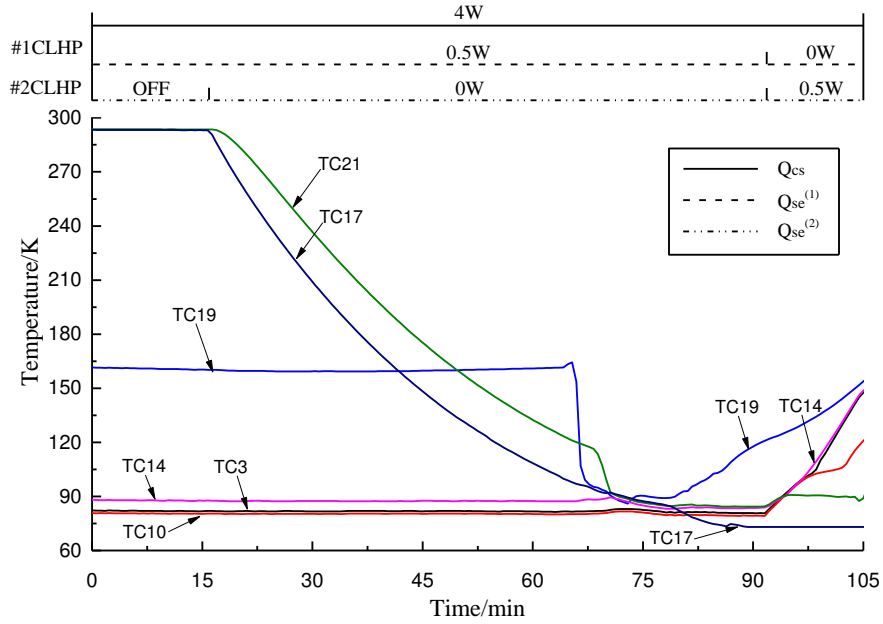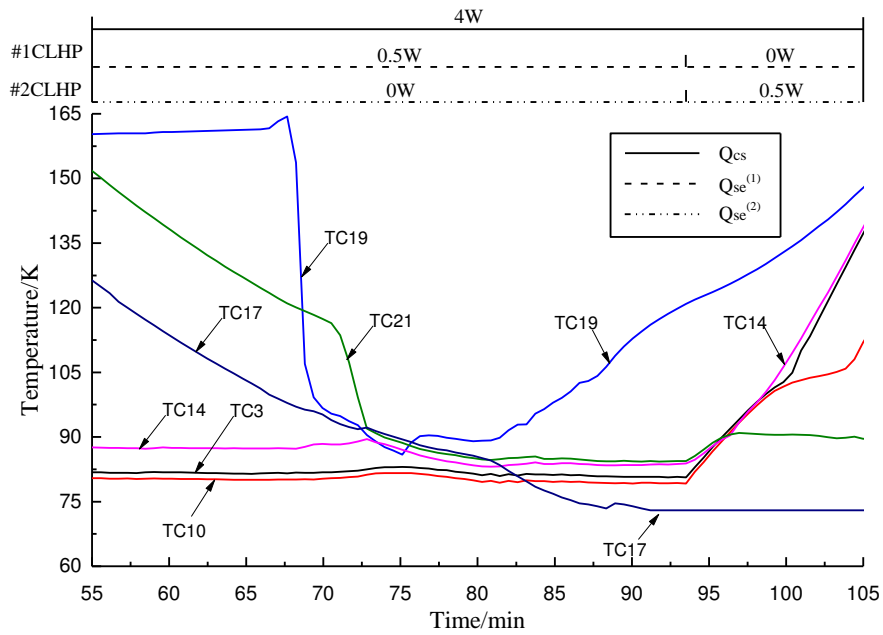
(a) the whole range

(b) local enlargement

Fig. 7 Supercritical startup process without auxiliary operation in the backup conversion mode
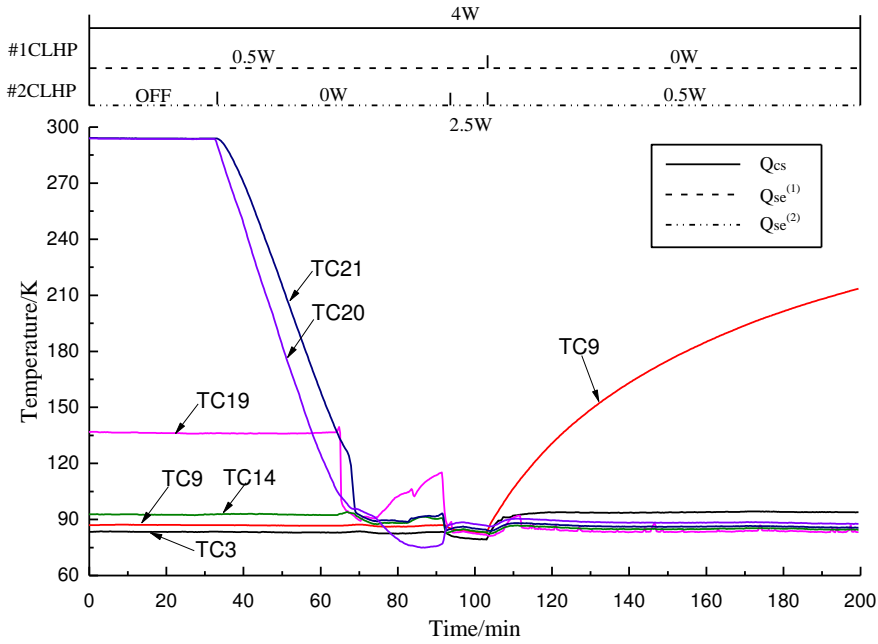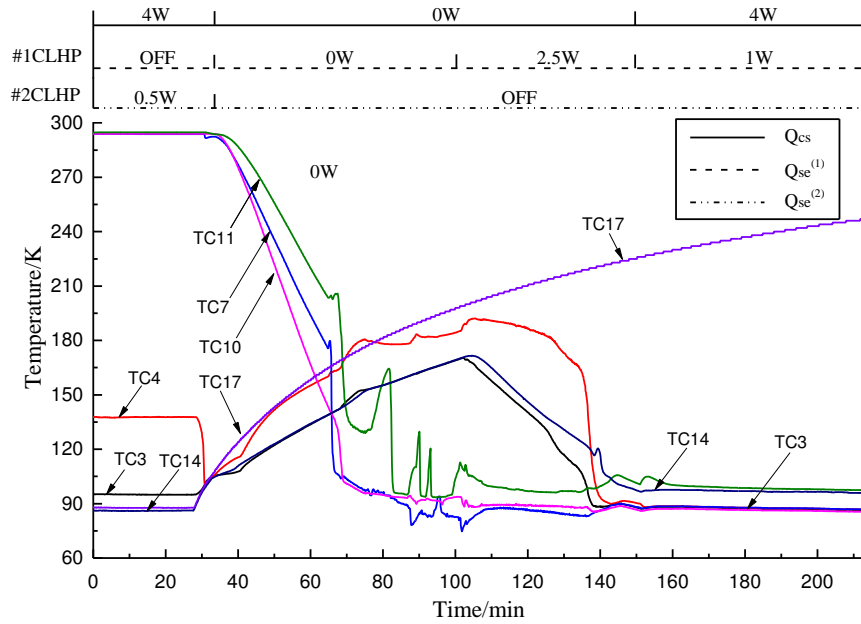
543

544 (a) the whole range
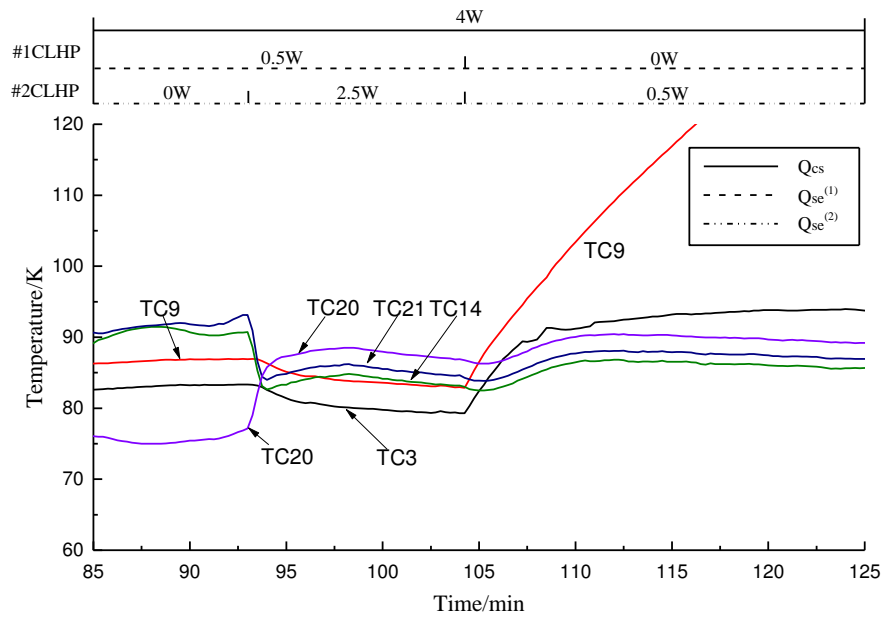
545

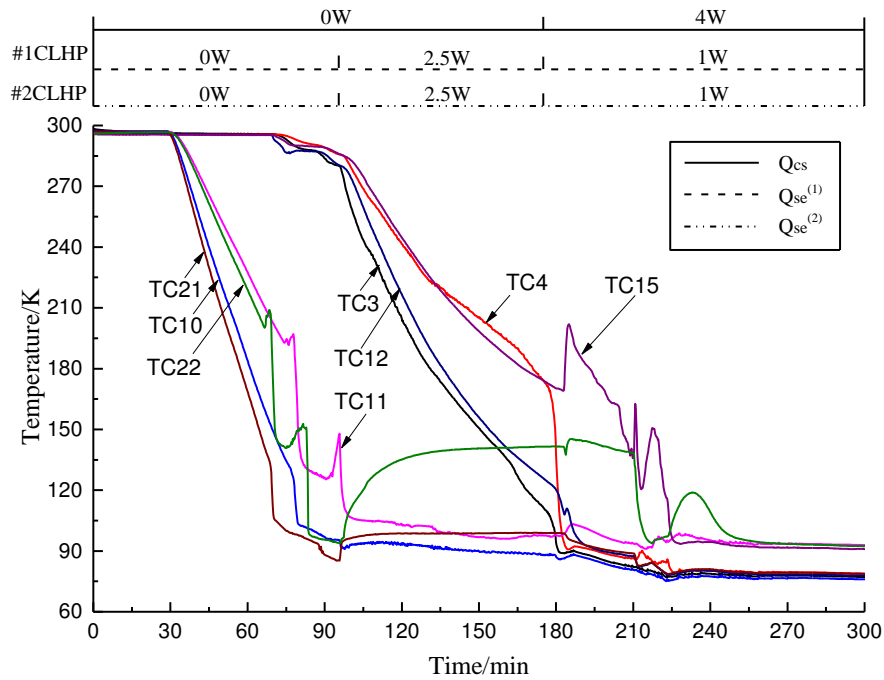546 (b) local enlargement

547 Fig. 8 Supercritical startup process with auxiliary operation in the backup conversion mode

548

549

550

551

552

553

554
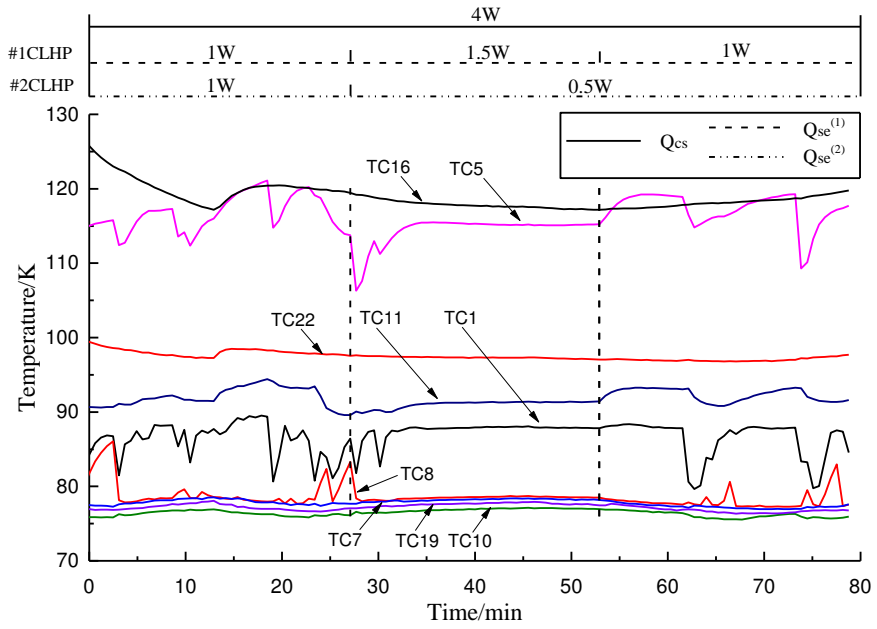
Fig. 9 Supercritical startup process in the malfunction conversion mode

556

557

Fig. 10 Supercritical startup process in the dual operation mode

558

559

560

561

562

563

Fig.11 Temperature oscillation phenomenon in the dual operation mode

566

567

568